

## Thin-layer black phosphorus/GaAs heterojunction p-n diodes

Pascal Gehring, Roberto Urcuyo, Dinh Loc Duong, Marko Burghard', and Klaus Kern

Citation: *Appl. Phys. Lett.* **106**, 233110 (2015); doi: 10.1063/1.4922531

View online: <http://dx.doi.org/10.1063/1.4922531>

View Table of Contents: <http://aip.scitation.org/toc/apl/106/23>

Published by the [American Institute of Physics](#)

---

### Articles you may be interested in

[Electric field effect in ultrathin black phosphorus](#)

*Appl. Phys. Lett.* **104**, 103106103106 (2014); 10.1063/1.4868132

---



**FIND THE NEEDLE IN THE  
HIRING HAYSTACK**

POST JOBS AND REACH THOUSANDS OF  
QUALIFIED SCIENTISTS EACH MONTH.

PHYSICS TODAY | JOBS  
[WWW.PHYSICSTODAY.ORG/JOBS](http://WWW.PHYSICSTODAY.ORG/JOBS)

## Thin-layer black phosphorus/GaAs heterojunction p-n diodes

Pascal Gehring,<sup>1</sup> Roberto Urcuyo,<sup>1</sup> Dinh Loc Duong,<sup>1</sup> Marko Burghard,<sup>1,a)</sup> and Klaus Kern<sup>1,2</sup>

<sup>1</sup>Max Planck Institute for Solid State Research, Heisenbergstrasse 1, D-70569 Stuttgart, Germany

<sup>2</sup>Institut de Physique de la Matière Condensée, Ecole Polytechnique Fédérale de Lausanne, CH-1015 Lausanne, Switzerland

(Received 27 January 2015; accepted 3 June 2015; published online 11 June 2015; corrected 10 September 2015)

Owing to its high carrier mobility and thickness-tunable direct band gap, black phosphorus emerges as a promising component of optoelectronic devices. Here, we evaluate the device characteristics of p-n heterojunction diodes wherein thin black phosphorus layers are interfaced with an underlying, highly n-doped GaAs substrate. The p-n heterojunctions exhibit close-to-ideal diode behavior at low bias, while under illumination they display a photoresponse that is evenly distributed over the entire junction area, with an external quantum efficiency of up to 10% at zero bias. Moreover, the observed maximum open circuit voltage of 0.6 V is consistent with the band gap estimated for a black phosphorus sheet with a thickness on the order of 10 nm. Further analysis reveals that the device performance is limited by the structural quality of the black phosphorus surface. © 2015 AIP Publishing LLC. [<http://dx.doi.org/10.1063/1.4922531>]

Two-dimensional (2D) layered materials like graphene and transition metal dichalcogenides (TMDCs) have made tremendous impact in the field of nanotechnology.<sup>1–8</sup> This has stimulated the development of a new generation of electronic devices including ultrathin field-effect transistors (FETs)<sup>3</sup> and optoelectronic devices like photodetectors,<sup>7,9–12</sup> spin-optoelectronic,<sup>8,13</sup> and optical modulators.<sup>14,15</sup> However, the zero band gap of graphene and the only modest carrier mobility of TMDCs pose serious hurdles toward electronic device applications. As an alternative 2D material, phosphorene (monolayer black phosphorus) has recently attracted strong interest due to its thickness-tunable, direct band gap, and high carrier mobility.<sup>16–20</sup> A range of corresponding electronic devices has been implemented, most prominently FETs,<sup>16,21</sup> inverters,<sup>18</sup> as well as phototransistors/detectors.<sup>22</sup> Furthermore, combining the p-type phosphorene with a monolayer of the n-type TMDC molybdenum disulfide (MoS<sub>2</sub>) has enabled photodetectors with sizable responsivity.<sup>23</sup> Phosphorene also shows promise as a component of solar energy harvesting devices, as documented by theoretical studies predicting that phosphorene bilayer-based solar cells enable an external quantum efficiency (EQE) of up to 18%.<sup>20</sup> In the present work, we investigate the photovoltaic behavior of p-n heterojunction diodes composed of a few tens of nm thick black phosphorus flakes on top of a highly n-doped GaAs substrate. The devices obtained in this manner attain an EQE that readily competes with that of very recently realized TMDC-based atomically thin p-n junctions.<sup>10,11</sup>

The thin-layer black phosphorus/GaAs p-n heterojunction devices were fabricated in four steps (see Fig. 1(a)). Initially, Te-doped n<sup>+</sup>-GaAs substrates ( $N_D^{GaAs} \approx 10^{24} \text{ m}^{-3}$ ) were first cleaned/etched and then provided with AuGeNi contacts using standard e-beam lithography and thermal evaporation.<sup>24</sup> Subsequently, the samples were annealed in

order to diffuse and alloy the contact material into the GaAs substrate, and thus achieve Ohmic contacts. In the second step, immediately after additional cleaning/etching of the GaAs surface to remove native oxides, thin black phosphorus flakes were exfoliated on top from a bulk crystal (Smart Elements, Vienna, Austria) using the Scotch tape method. We observed black phosphorus flakes with lateral size up to several  $\mu\text{m}$  and thickness down to 10 nm. Separate electrical measurements on individual such flakes confirmed their p-type behavior.<sup>24</sup> The third step involved thermal evaporation of a 100 nm thick SiO<sub>x</sub> film at the contact regions, in order to avoid the formation of a trivial Schottky barrier between the electrical contacts to phosphorene and the underlying GaAs substrate. In the last step, the black phosphorus flakes and AuGeNi anchor points (closest to the flakes) were electrically contacted via e-beam lithography and thermal evaporation of 60 nm Ni/90 nm Au. Figs. 1(e) and 1(f) display a schematic of the cross-section and an optical micrograph of a typical device, respectively. To prevent degradation of the black phosphorus under ambient, a 50 nm thick film of PMMA was spin-coated onto the substrate directly after the lift-off procedure.

In Fig. 2, the band alignment of the n-GaAs/p-black phosphorus heterostructure, as derived from the Anderson model of semiconductor heterojunctions,<sup>25</sup> is schematically illustrated. For the work function of the heavily n-doped GaAs, we assume a value of approximately 4.1 eV, close to the electron affinity of the intrinsic material. As the band gap and work function of the black phosphorus both depend sensitively on the flake thickness, we used the numerical values for ten layers of phosphorene of  $\Phi_{bP} = 4.5 \text{ eV}$ ,  $\chi_{bP} = 4.13 \text{ eV}$ , and  $E_g^{bP} = 0.6 \text{ eV}$ , which should be valid for layers with a thickness of several tens of nm.<sup>17,26</sup> Based upon these values, one calculates a built-in electric potential of  $V_{bi} = \Phi_{bP} - \Phi_{GaAs} = 0.44 \text{ eV}$ , a conduction band offset of  $\Delta E_c = \chi_{bP} - \chi_{GaAs} = 0.06 \text{ eV}$ , and a valence band offset of  $\Delta E_v = (\chi_{GaAs} + E_g^{GaAs}) - (\chi_{bP} + E_g^{bP}) = -0.78 \text{ eV}$ .

<sup>a)</sup>Electronic mail: m.burghard@fkf.mpg.de

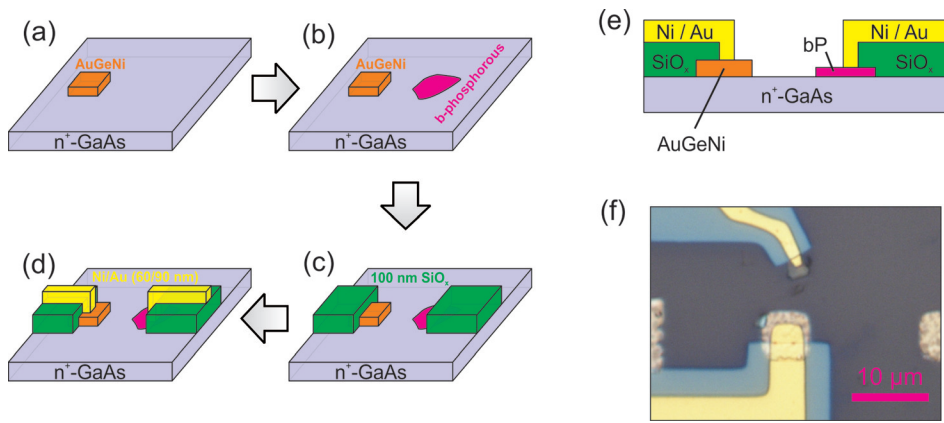


FIG. 1. (a)-(d) Schematic representation of the fabrications steps for the thin layer black phosphorus/GaAs p-n heterojunction devices. (e) Sketch of the cross-section of a completed device, and (f) optical micrograph of a heterojunction device (top view).

The output characteristic of the device described above (Fig. 1(f)), where the contact to n-doped GaAs is used as source and the contact to p-doped black phosphorus as drain, is shown in Fig. 2(b) for the  $V_{sd}$  range of  $-1$  to  $+1$  V. The asymmetric  $I$ - $V$  curve signifies typical rectification behavior in linear and log scale (inset) as expected for a p-n junction. The asymmetry  $\frac{I_{sd}(V)}{I_{sd}(-V)}$  and the nonlinearity  $\frac{dI/dV}{I/V}$  extracted from this curve are plotted in Fig. 2(c).<sup>27</sup> For this specific device, the rectification ratio (=asymmetry) is 120 at a bias of 1 V. From the entire set of investigated devices, we determined rectification ratios between 100 and 1000. Such notable variation most likely originates from variations in both, the black phosphorus flake thickness and the active device area (corresponding to a different area to edge ratio of the heterostructures).<sup>28</sup> In addition, the fabrication process itself might slightly change the device characteristics, since black phosphorus is chemically quite sensitive against ambient.<sup>29</sup> Another important parameter that can be extracted from the  $I$ - $V$  characteristic of the diodes is the ideality factor  $n$  which provides useful information about charge transport mechanism as well as the device quality.<sup>30</sup> Fig. 2(d) displays the

effective saturation current  $I_0^{eff}$  along with the effective ideality factor  $n_{eff}$  of the above device, as extracted from the  $I$ - $V$  curve using  $I_{sd} = I_0^{eff} \exp\left(\frac{V_{sd}}{n_{eff} k_B T} - 1\right) - I_{pc}$ , where  $I_{pc}$  is the photocurrent. Both these parameters contain contributions of a recombination current and Ohmic shunt (parallel to the diode) and series resistances. At low bias,  $n_{eff}$  is found to be close to 2, the theoretical value for an ideal diode where only recombination currents occur at the junction. Upon increasing the bias,  $n_{eff}$  reaches a maximum value of 9.7 (at 0.8 V). Such high value indicates strong recombination due to defects,<sup>28,31</sup> which might comprise intrinsic point defects inside the black phosphorus, surface defects on it arising from chemical degradation, or due to a bad contact between black phosphorus and GaAs. Another explanation involves the presence of an alternative transport channel (shunt resistance). In the high bias regime (above 0.8 V), the ideality factor decreases again as a consequence of the increased diffusion current.

The p-n diode behavior of the devices could be further confirmed by scanning photocurrent microscopy measurements. Figs. 3(a) and 3(b), respectively, depict an optical

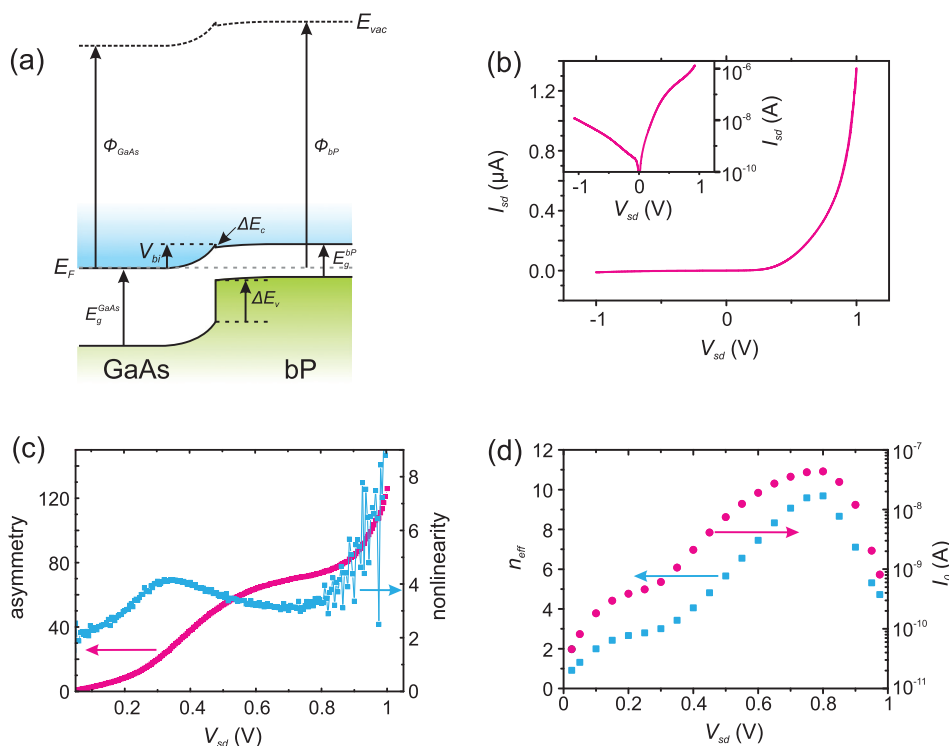


FIG. 2. (a) Schematic depiction of the band alignment at the black phosphorus/ $n^+$ -GaAs heterojunction, constructed using Anderson's model. The valence and conduction band are colored in green and blue, respectively. (b) Room temperature  $I$ - $V$  characteristic in linear and log scale (inset) of the device in Figure 1(f). (c) Asymmetry (pink) and nonlinearity (blue) of the device as a function of forward bias. (d) Effective ideality factor and effective saturation current extracted from fits of the  $I$ - $V$  characteristic (window size of the individual fits: 100 mV).

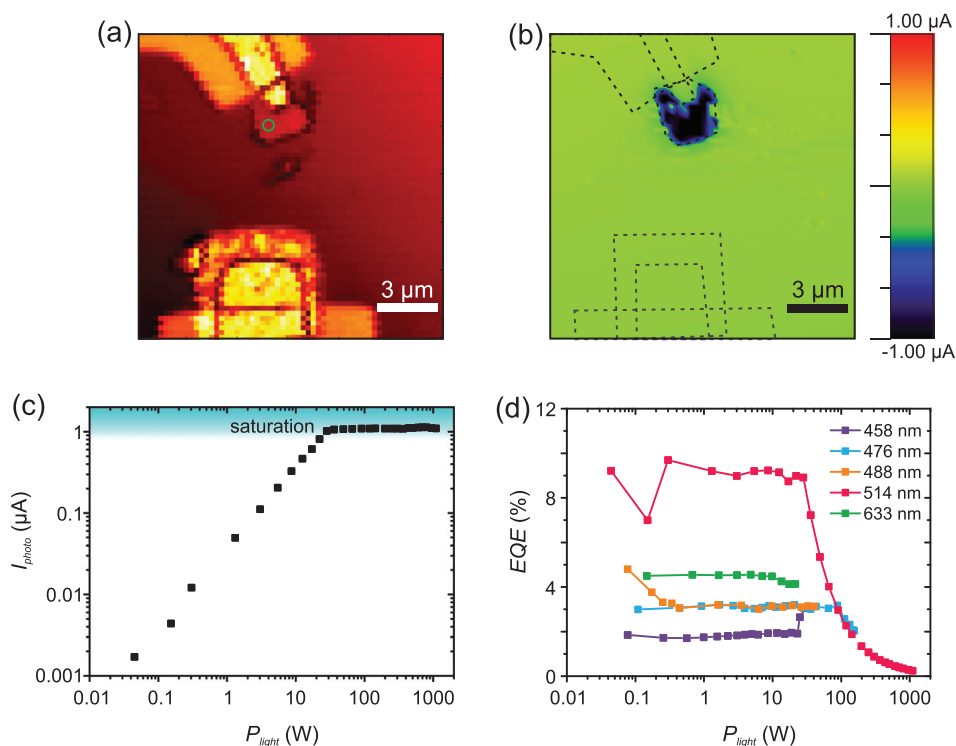


FIG. 3. (a) Optical reflection image and (b) photocurrent map of the device in Figure 1(f), recorded at zero source-drain bias. (c) Photocurrent as a function of laser power at  $\lambda = 514$  nm. The signal was acquired from the green circle in panel (a). The blue shaded region visualize current saturation. (d) EQE as a function of laser power for different laser light wavelengths.

reflection image and photocurrent map of the above device, recorded at  $V_{sd} = 0$  V using a laser wavelength of 514 nm and a laser power of  $36 \mu\text{W}$ . It is evident that efficient charge carrier separation and thus photocurrent generation exclusively occur at the region, where the black phosphorus flake and the underlying GaAs substrate form a heterojunction. The negative sign of the photocurrent is in accord with the corresponding band diagram in Fig. 2(b). Moreover, the uniformity of photocurrent over the whole black phosphorus region even near the Ni/Au contact, combined with the absence of photocurrent generation at the AuGeNi contact to GaAs, prove that the asymmetric I-V characteristic originates from a real p-n junction rather than Schottky barriers at the contacts to the individual semiconducting components. In the latter case, a gradual decrease of photocurrent with increasing distance from the contact is commonly observed.<sup>32</sup> Although a (small) Schottky barrier might exist between Ni/Au and black phosphorus, the overall photocurrent signal is clearly dominated by the signal located at the p-n junction.<sup>24</sup>

The dependence of photocurrent on light power is illustrated in Fig. 3(c), which plots the maximum photocurrent of the same device extracted from individual zero-bias photocurrent maps recorded at different light powers. The linear increase of photocurrent with increasing light power is in agreement with the established behavior of photodiodes. From a linear data fit, one obtains a responsivity  $R = I_{pc}/P_{light}$  of 37 mA/W (at zero bias and  $\lambda = 514$  nm), comparable to values reported for bP/MoS<sub>2</sub> or CNT/MoS<sub>2</sub> heterojunctions, although the latter were recorded under sizable bias.<sup>23,33</sup> Above approximately  $30 \mu\text{W}$ , the photocurrent abruptly flattens (at about  $1.1 \mu\text{A}$ ) owing to the saturated optical absorption of the black phosphorus flake at high light intensities. In the present device, due to the very high doping level of the GaAs, the space charge region is mostly confined

to the black phosphorus layer, whereas only a very thin positive space charge region exists in GaAs.<sup>24</sup> Hence, the magnitude of the photocurrent is mainly governed by the number of available charge carriers inside the black phosphorus flake. Another reason is screening by the photo-generated carriers which eliminates the bias across the depletion layer.<sup>34</sup>

The photo-response of the device exhibits a clear wavelength dependence, as evident from Fig. 3(d), which plots the external quantum efficiency  $EQE = \frac{I_{pc}}{P_{light}} \cdot \frac{hc}{e\lambda}$  (where  $h$  is the Planck constant,  $c$  is the speed of light,  $e$  is the elementary charge, and  $\lambda$  is the laser wavelength) at zero bias as a function of light power and laser wavelength. The EQE reaches a maximum value of 9.7% for  $\lambda = 514$  nm, which is of the same order of magnitude as reported for atomically thin TMDC heterostructures.<sup>9–11</sup> For higher light power, the efficiency drops drastically due to the current saturation effect apparent in Fig. 3(c). The observation of maximum EQE at  $\lambda = 514$  nm is consistent with the reported behavior of pure black phosphorus pn-junctions and is attributable to enhanced optical absorption around this wavelength arising from van Hove singularities in the joint density of states.<sup>35</sup>

Toward evaluating the bias dependence of the EQE, we recorded photocurrent maps at different bias voltages for a constant light power of  $8.6 \mu\text{W}$  and a laser wavelength of 514 nm. Thus gained EQE values (Fig. 4) monotonously increase upon application of an increasing reverse bias, as expected from the enhanced band bending and the size of the depletion layer. As a consequence, at an applied bias voltage of  $-1$  V the EQE doubles compared to zero bias. By comparison, application of an increasing forward bias flattens out the band bending, such that the photocurrent decreases significantly. This trend continues until the flat-band situation is reached at approximately  $V_{fb} = 0.6$  V. Upon further increasing the forward bias, the applied voltage drops over the

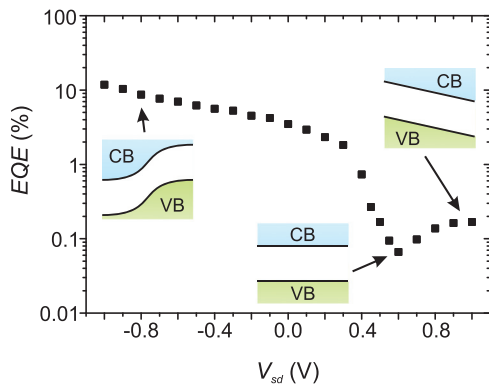


FIG. 4. EQE under illumination with  $\lambda = 514\text{ nm}$ , plotted as a function of source-drain bias voltage. The maximum photocurrent was extracted from individual photocurrent maps recorded at different bias voltages. In the inset, the crossover from a p-n junction to flat bands to normal resistive behavior is indicated by corresponding band alignments.

entire device, whereupon the photocurrent sign changes and the EQE increases again.<sup>24</sup> Within the entire set of investigated devices, we observed EQE values of up to 31% at a bias of  $-2.5\text{ V}$ .<sup>24</sup>

We further explored the photovoltaic characteristic of the black phosphorus/GaAs p-n heterojunctions. Fig. 5(a) compares I-V traces of the above device for different laser powers ( $\lambda = 514\text{ nm}$ ) recorded with the laser spot at a fixed position (green circle in Fig. 3(a)). Upon increasing the light power, both the short circuit current  $I_{sc}$  as well as the open circuit voltage  $V_{oc}$  can be seen to first increase and then to saturate. This behavior reproduces the laser power dependence in Fig. 3(c). The maximum open circuit voltage of  $\sim 0.6\text{ V}$  corresponds well to the estimated band gap of  $\sim 0.56\text{ eV}$  for the present black phosphorus sheet, whose thickness was determined to be  $\sim 15\text{ nm}$  by AFM analysis.<sup>24,26</sup> It is noteworthy that the experimental transport band gap of

phosphorene with the same thickness is smaller than this estimate.<sup>36</sup> In Fig. 5(b), the electrical power  $P_{el} = V_{sd} \cdot I_{sd}$  is plotted as a function of the applied bias for the corresponding laser powers. In conjunction with the open circuit voltages  $V_{oc}$  (see inset of Fig. 5(c)) and the short circuit currents  $I_{sc}$ , a maximum fill factor  $FF = \frac{P_{el}}{V_{oc} \cdot I_{sc}} = 0.3$  is obtained for this device. This value is inferior to the typical range of 0.5–0.8 documented for conventional solar cells.<sup>37</sup> Closer analysis reveals that this difference results from a low shunt resistance  $R_{sh}$  combined with a high series resistance  $R_s$  in the present devices.<sup>24,38</sup> The former testifies the presence of an alternative current path for the photo-excited electron-hole pairs, such as charge transport through a Schottky barrier between the metal contact to black phosphorus and the underlying GaAs (formed due to possible imperfections in the  $\text{SiO}_x$ ). The high series resistance, on the other hand, is a direct consequence of the quite high contact resistance between Ni/Au and black phosphorus.<sup>24</sup> In fact, we observed a two-point resistance in the  $\text{M}\Omega$  range for black phosphorus flakes, whereas values on the order of tens of  $\text{k}\Omega$  have been reported by others.<sup>19</sup> The origin of the non-optimal contacts in our devices remains to be clarified, although the surface instability of the black phosphorus is most likely involved. The above scenarios are consistent with our fitting model of the dark current, where the extracted ideality factor is significantly higher than expected for an ideal p-n junction.

In Fig. 5(c), the open circuit voltage  $V_{oc}$  of the above device is shown in dependence of the short circuit current  $I_{sc}$ . Theoretically, the open circuit voltage  $V_{oc}$  should increase with the light-generated current  $I_L$  ( $\approx I_{sc}$ ) according to  $V_{oc} = \frac{nkT}{q} \ln\left(\frac{I_L}{I_0} + 1\right)$ . The pink curve in Fig. 5(c) represents a data fit based on this model, which yields an ideality factor of  $n = 2.3$  and a saturation current  $I_0 = 0.17\text{ nA}$ . Both these values coincide very well with those extracted from the I-V

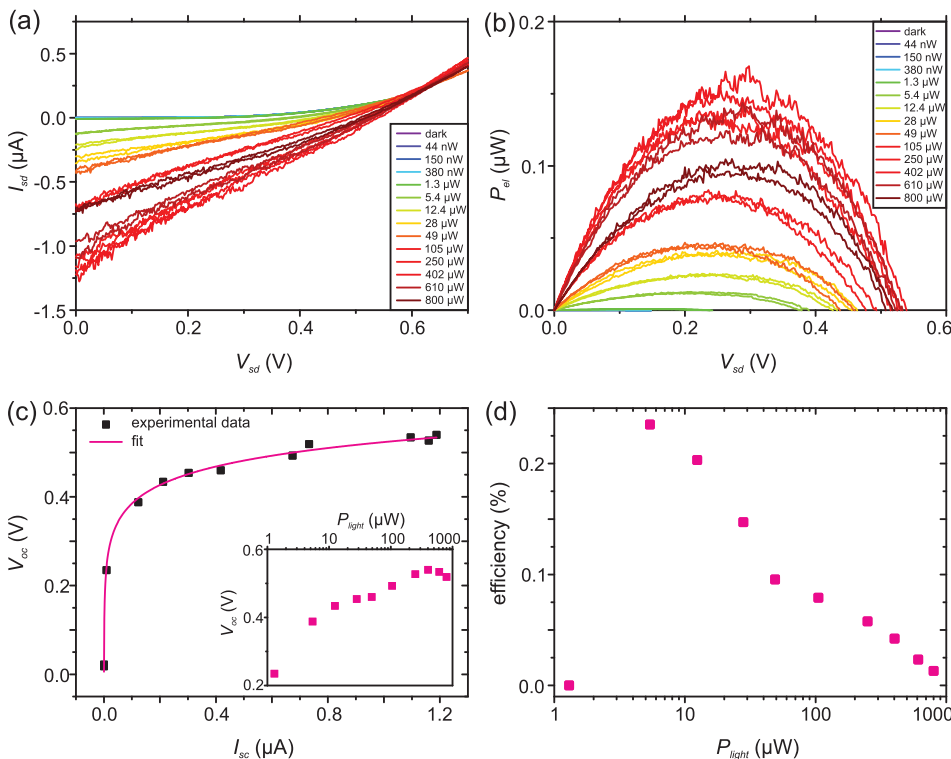


FIG. 5. (a) I-V curves and (b) corresponding electrical power output of the device depicted in Figure 1(f) for different laser powers ( $\lambda = 514\text{ nm}$ ). The signal was recorded from the green circle in Figure 3(a). (c) Open circuit voltage as a function of short circuit current derived from the plot in panel (a). The pink curve is a data fit. Inset: Open circuit voltage in dependence of light power. (d) Photoconversion efficiency of the device as a function of light power. The deviation of the data point at lowest laser power is due to the limited resolution in these measurements.

curves in the low bias regime (see Fig. 2(d)). Furthermore, based upon the maximum electrical power  $P_{el,max}$  for different laser powers  $P_{light}$  the photoconversion efficiency  $P_{el,max}/P_{light}$  can be calculated. It features a maximum of 0.24% and decreases notably with increasing laser power (see Fig. 5(d)), comparable to the performance of van der Waals heterojunctions composed of ultrathin layers of black phosphorus and molybdenum disulfide ( $\text{MoS}_2$ ).<sup>23</sup>

In summary, our p-n heterojunction diodes comprising thin layers of black phosphorus as the p-type component display pronounced rectification behavior which in the low bias regime approaches that of ideal diodes. Moreover, when operated as photodiodes, they reach external quantum efficiencies of upto 10% under zero bias, and more than 30% under higher reverse bias. Despite these impressive values, the device performance is still limited, as reflected by a quite low fill factor ( $<0.3$ ), as well as an only moderate electrical power output. Enhanced device performance can be expected from a better control of the chemical nature of the black phosphorus surface, complemented by the implementation of improved electrical contacts.

R.U. acknowledges the Universidad de Costa Rica for providing a doctoral exchange scholarship.

- <sup>1</sup>A. K. Geim and I. V. Grigorieva, *Nature* **499**, 419 (2013).
- <sup>2</sup>F. Schwierz, *Nat. Nanotechnol.* **5**, 487 (2010).
- <sup>3</sup>G. Fiori, F. Bonaccorso, G. Iannaccone, T. Palacios, D. Neumaier, A. Seabaugh, S. K. Banerjee, and L. Colombo, *Nat. Nanotechnol.* **9**, 768 (2014).
- <sup>4</sup>K. S. Novoselov, V. I. Fal'ko, L. Colombo, P. R. Gellert, M. G. Schwab, and K. Kim, *Nature* **490**, 192 (2012).
- <sup>5</sup>K. Kim, J.-Y. Choi, T. Kim, S.-H. Cho, and H.-J. Chung, *Nature* **479**, 338 (2011).
- <sup>6</sup>Q. H. Wang, K. Kalantar-Zadeh, A. Kis, J. N. Coleman, and M. S. Strano, *Nat. Nanotechnol.* **7**, 699 (2012).
- <sup>7</sup>F. H. L. Koppens, T. Mueller, P. Avouris, A. C. Ferrari, M. S. Vitiello, and M. Polini, *Nat. Nanotechnol.* **9**, 780 (2014).
- <sup>8</sup>X. Xu, W. Yao, D. Xiao, and T. F. Heinz, *Nat. Phys.* **10**, 343 (2014).
- <sup>9</sup>C.-H. Lee, G.-H. Lee, A. M. van der Zande, W. Chen, Y. Li, M. Han, X. Cui, G. Arefe, C. Nuckolls, T. F. Heinz, J. Guo, J. Hone, and P. Kim, *Nat. Nanotechnol.* **9**, 676 (2014).
- <sup>10</sup>B. W. H. Baugher, H. O. H. Churchill, Y. Yang, and P. Jarillo-Herrero, *Nat. Nanotechnol.* **9**, 262 (2014).
- <sup>11</sup>A. Pospischil, M. M. Furchi, and T. Mueller, *Nat. Nanotechnol.* **9**, 257 (2014).
- <sup>12</sup>H. Fang, C. Battaglia, C. Carraro, S. Nemsak, B. Ozdol, J. S. Kang, H. A. Bechtel, S. B. Desai, F. Kronast, A. A. Unal, G. Conti, C. Conlon, G. K. Palsson, M. C. Martin, A. M. Minor, C. S. Fadley, E. Yablonovitch, R. Maboudian, and A. Javey, *Proc. Natl. Acad. Sci. U. S. A.* **111**, 6198 (2014).
- <sup>13</sup>H. Yuan, X. Wang, B. Lian, H. Zhang, X. Fang, B. Shen, G. Xu, Y. Xu, S.-C. Zhang, H. Y. Hwang, and Y. Cui, *Nat. Nanotechnol.* **9**, 851 (2014).
- <sup>14</sup>M. Liu, X. Yin, E. Ulin-Avila, B. Geng, T. Zentgraf, L. Ju, F. Wang, and X. Zhang, *Nature* **474**, 64 (2011).
- <sup>15</sup>J. S. Ross, P. Klement, A. M. Jones, N. J. Ghimire, J. Yan, D. G. Mandrus, T. Taniguchi, K. Watanabe, K. Kitamura, W. Yao, D. H. Cobden, and X. Xu, *Nat. Nanotechnol.* **9**, 268 (2014).
- <sup>16</sup>L. Li, Y. Yu, G. J. Ye, Q. Ge, X. Ou, H. Wu, D. Feng, X. H. Chen, and Y. Zhang, *Nat. Nanotechnol.* **9**, 372 (2014).
- <sup>17</sup>Y. Cai, G. Zhang, and Y.-W. Zhang, *Sci. Rep.* **4**, 6677 (2014).
- <sup>18</sup>H. Liu, A. T. Neal, Z. Zhu, Z. Luo, X. Xu, D. Tománek, and P. D. Ye, *ACS Nano* **8**, 4033 (2014).
- <sup>19</sup>H. Liu, Y. Du, Y. Deng, and P. D. Ye, *Chem. Soc. Rev.* **44**, 2732 (2015).
- <sup>20</sup>J. Dai and X. Zeng, *J. Phys. Chem. Lett.* **5**, 1289 (2014).
- <sup>21</sup>H. Liu, A. Neal, M. Si, Y. Du, and P. Ye, *IEEE Electron Dev. Lett.* **35**, 795 (2014).
- <sup>22</sup>M. Buscema, D. J. Groenendijk, G. A. Steele, H. S. J. van der Zant, and A. Castellanos-Gomez, *Nat. Commun.* **5**, 4651 (2014).
- <sup>23</sup>Y. Deng, Z. Luo, N. J. Conrad, H. Liu, Y. Gong, S. Najmaei, P. M. Ajayan, J. Lou, X. Xu, and P. D. Ye, *ACS Nano* **8**, 8292 (2014).
- <sup>24</sup>See supplemental material at <http://dx.doi.org/10.1063/1.4922531> for device fabrication details, the electrical characterization of bare phosphorene, the estimation of the depletion layer thickness, the extraction of shunt and series resistance, the gate dependence of the photocurrent around the flat band situation, and a height profile of the phosphorene sheet.
- <sup>25</sup>R. L. Anderson, *IBM J. Res. Dev.* **4**, 283 (1960).
- <sup>26</sup>V. Tran, R. Soklaski, Y. Liang, and L. Yang, *Phys. Rev. B* **89**, 235319 (2014).
- <sup>27</sup>P. Periasamy, H. L. Guthrey, A. I. Abdulagatov, P. F. Ndione, J. J. Berry, D. S. Ginley, S. M. George, P. A. Parilla, and R. P. O'Hayre, *Adv. Mater.* **25**, 1301 (2013).
- <sup>28</sup>O. Breitenstein, *Opto-Electron. Rev.* **21**, 259 (2013).
- <sup>29</sup>C.-G. Andres, V. Leonardo, P. Elsa, O. I. Joshua, K. L. Narasimha-Acharya, I. B. Sofya, J. G. Dirk, B. Michele, A. S. Gary, J. V. Alvarez, W. Z. Henny, J. J. Palacios, and S. J. V. D. Z. Herre, *2D Mater.* **1**, 025001 (2014).
- <sup>30</sup>K. K. N. S. M. Sze, *Physics of Semiconductor Devices* (Wiley, 2007).
- <sup>31</sup>O. Breitenstein, *Advances in Photovoltaics: Part 2* (Elsevier, 2013).
- <sup>32</sup>F. Xia, T. Mueller, R. Golizadeh-Mojarad, M. Freitag, Y. Lin, J. Tsang, V. Perebeinos, and P. Avouris, *Nano Lett.* **9**, 1039 (2009).
- <sup>33</sup>D. Jariwala, V. K. Sangwan, C.-C. Wu, P. L. Prabhuramirashi, M. L. Geier, T. J. Marks, L. J. Lauhon, and M. C. Hersam, *Proc. Natl. Acad. Sci. U. S. A.* **110**, 18076 (2013).
- <sup>34</sup>Z. Li, Y. Fu, M. Piels, H. Pan, A. Beling, J. E. Bowers, and J. C. Campbell, *Opt. Express* **19**, B385 (2011).
- <sup>35</sup>H. Yuan, X. Liu, F. Afshinmanesh, W. Li, G. Xu, J. Sun, B. Lian, A. G. Curto, G. Ye, Y. Hikita, Z. Shen, S.-C. Zhang, X. Chen, M. Brongersma, H. Y. Hwang, and Y. Cui, "Polarization-sensitive broadband photodetector using a black phosphorus vertical p-n junction," *Nat. Nanotechnol.* (published online).
- <sup>36</sup>S. Das, W. Zhang, and M. Demarteau, *Nano Lett.* **14**, 5733 (2014).
- <sup>37</sup>B. Qi and J. Wang, *Phys. Chem. Chem. Phys.* **15**, 8972 (2013).
- <sup>38</sup>O. Breitenstein, J. Bauer, P. P. Altermatt, and K. Ramspeck, *Solid State Phenom.* **156-158**, 1 (2009).